STUDY ON THE PERFORMANCE IMPROVEMENT OF PEMFC BY MAGIC MANTIS PSEUDO SNAKE PLATE

Baohua LI[1], Rui LI[2],Yuanjun DAI[3]

In this paper, a magic mantis pseudo snake plate is designed, and a three dimensional, steady state, isothermal multiphase proton exchange membrane fuel cell model is used for fluent simulation. Comparing the magic mantis pseudo snake plate with different flow channel sections of the same flow channel volume with the traditional single snake plate, the results show that the volume of the bipolar plate is reduced by 46.74 %. The peak power of the fuel cell of the magic mantis pseudo snake plate with a pentagonal flow channel section is increased by 23.64 %, and the peak current is increased by 33.23 %.

Keywords: proton exchange membrane fuel cell; fluent simulation; flow channel

1 Introduction

With the promulgation of the national comprehensive work plan for energy conservation and emission reduction, all parts of the country have begun to formulate corresponding measures to help New China achieve a ' zero carbon ' society as soon as possible. The proton exchange membrane fuel cell directly converts chemical energy into electrical energy through internal electrochemical reactions. The thermal efficiency is about 23%~34% higher than the thermal efficiency of the Carnot heat engine. Its advantages are obvious. First, it is efficient and clean, does not emit harmful substances, and therefore does not pollute the environment. Secondly, there is no noise during operation, which can reduce noise pollution. In addition, proton exchange membrane fuel cells also have the potential for renewable energy storage and utilization. In summary, proton exchange membrane fuel cell is a new type of energy equipment with high efficiency and low noise, and also has the advantage of using renewable energy. Therefore, proton exchange membrane fuel cells are widely used in automobiles, ships, aircraft, household energy and other fields. Designing a suitable bipolar

[1] A.P., Mechanical Engineering Institute, Shanghai Dianji University, Shanghai, email: 764500870@qq.com

[2] Postgraduate., Mechanical Engineering Institute, Shanghai Dianji University, Shanghai, email: 33818146@qq.com

[3] Prof., Mechanical Engineering Institute, Shanghai Dianji University, Shanghai, email: 24354267@qq.com

plate is one of the important factors to reduce the cost and improve the performance of PEMFC stack.[1],Different types of plates are used for different usage scenarios to achieve maximum power[2]. Zou Yuting et al.[3]optimized the flow field of a ten channel serpentine plate by adding a shunt. The inlet flow channel was grouped by grouping and merging design. Once the gas reached the outlet area, the grouped flow channels were merged, which not only increased the internal pressure of the shunt, but also balanced the material concentration distribution in the inlet and outlet areas. Xuan et al.[4] proposed a microstructured lotus shaped plate flow channel. By optimizing the height, pore size and spacing of different microstructures, the liquid water in the flow channel is effectively discharged from the wall and its transport efficiency is accelerated.Based on the construction theory and Murray 's law, Qiong et al.[5]constructed a plate flow field that can effectively reduce parasitic losses to achieve the purpose of system energy saving. Huang et al.[6]used genetic algorithm to set the top and bottom edge widths of the anode and cathode channels as independent variables to optimize the channel cross section to achieve better mass transfer performance and avoid greater pressure drop loss. Fan et al. [7]found that the pore shape has a significant effect on the critical volume and growth period of the droplet by studying the influence of the pore shape and spacing inside the plate channel on the liquid water.

Based on the above content, it can be seen that in the fuel cell, the performance can be effectively improved by changing the structure of the bipolar plate. At present, it mainly focuses on optimizing the channel size, improving the smoothness of the channel wall and changing the channel material. The design of the shape structure of organisms through nature is rare. In this paper, the structure of the land creature magic flower mantis is selected as the inspiration source of bionic design. The structure has excellent flow characteristics, which can effectively enhance gas flow and improve mass transfer efficiency. A three dimensional, multiphase and isothermal numerical model was established for simulation research. By comparing the flow behavior of the reaction gas in the flow channel of the magic flower mantis pseudo snake plate and the serpentine plate with the same flow channel volume and different flow channel sections, the polarization curve of PEMFC, the distribution of oxygen and water in the cathode flow channel, the temperature distribution of the bipolar plate, the water distribution of the gas diffusion layer, the pressure drop of the flow channel and other parameters were analyzed. The performance difference between the magic flower mantis pseudo snake plate and the traditional serpentine plate with different cross section flow channels was obtained.

2 Numerical model

2.1 Three dimensional model

The tentacles on the head of the mantis are used to sense vibrations in the air, as well as the temperature and humidity. This helps the mantis perceive changes in its surroundings and adapt to different environments. In Fig. 1, we can see the established flow channel model, where the x direction represents the width of the battery, the y direction represents the length, and the z direction is perpendicular to the plate. The structure of the PEMFC (Proton Exchange Membrane Fuel Cell) from top to bottom includes the anode bipolar plate (BPP), anode flow channel, anode gas diffusion layer (GDL), anode catalytic layer (CL), proton exchange membrane (PEM), cathode CL, cathode GDL, cathode flow channel, and cathode BPP.

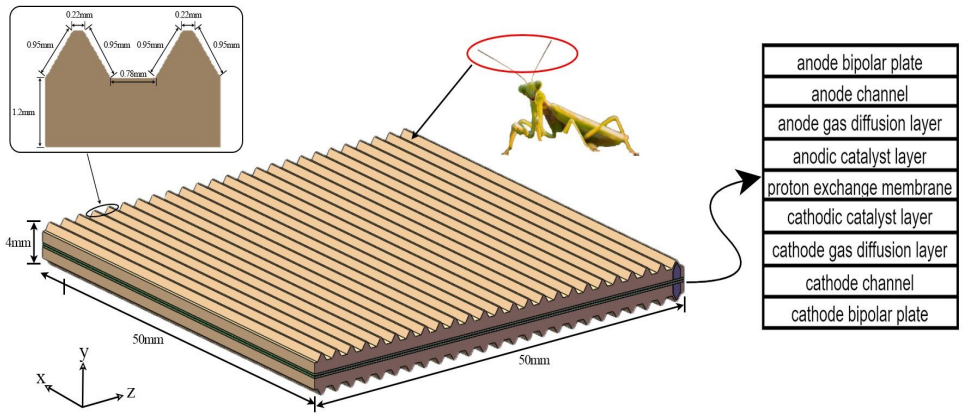

Fig. 1. PEMFC schematic diagram of magic mantis pseudo snake plate

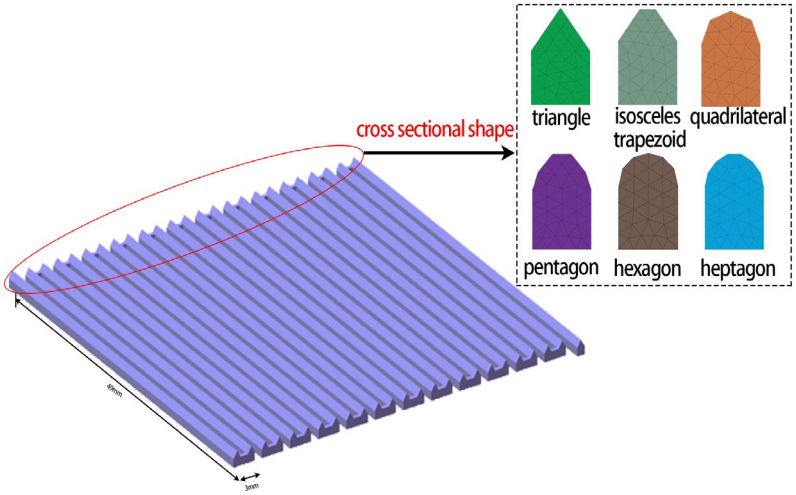

Fig. 2. The magic flower mantis pseudo snake plate gas flow channel

The flow channels for both the cathode and anode resemble a snake plate, as illustrated in Fig 2. Each flow channel has a single inlet and outlet position, as shown in the figure. Fig 3 provides the geometric parameters of the simulation model studied in this paper.

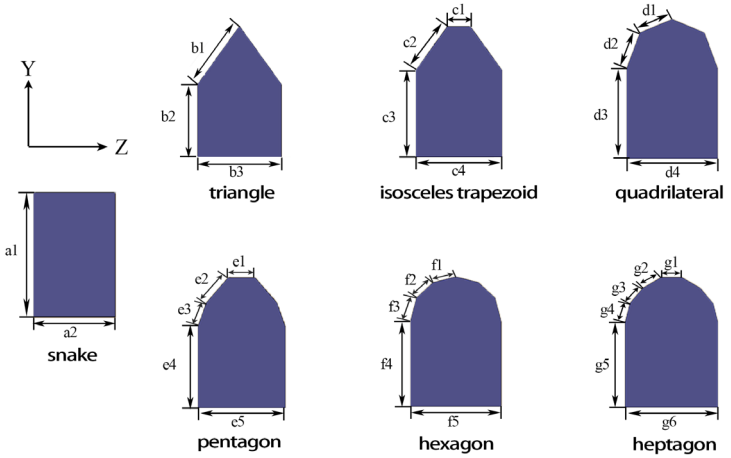

Fig. 3. Flow channel section size diagram

In order to study the performance difference of the pseudo snake plate of the magic flower mantis with different flow channel cross sections, six different shapes of flow channel cross sections were set up for analysis and compared with the serpentine plate flow channel. The size of the flow channel cross section is shown in Fig 3. In the serpentine plate flow channel cross section, a1 is 1.4mm, a2 is 1mm ; in the triangular section, b1 is 0.94mm, b2 is 1mm, b3 is 1mm ; in the isosceles trapezoid section, c1 is 0.27mm, c2 is 0.52mm, c3 is 1mm, c4 is 1mm ; in the quadrilateral section, d1 is 0.38mm, d2 is 0.43mm, d3 is 1mm, d4 is 1mm ; in the pentagonal section, e1 is 0.51 mm, e2 is 0.4 mm, e3 is 0.31 mm, e4 is 1 mm, e5 is 1 mm ; in the hexagonal section, f1 is 0.26 mm and f2 is 0.26 mm. f3 is 0.29mm, f4 is 1mm, f5 is 1mm ; in the heptagonal section, g1 is 0.22 mm, g2 is 0.24 mm, and g3 is 0.23 mm. g4 is 0.23mm, g5 is 1mm, g6 is 1mm.

2.2 Computation module

The three dimensional isothermal multiphase PEMFC numerical model in this study includes fluid flow, energy transfer, water transport, charge conservation, electron and proton transport equations. In order to facilitate numerical calculation and improve the efficiency of numerical simulation[8], the following assumptions and simplifications are made to the model:

1. The flow field in PEMFC is steady and isothermal, ignoring the time correlation.

2. The reaction gas flows into the reaction channel in a stable laminar flow.

3. The materials of proton exchange membrane, gas diffusion layer and catalytic layer are isotropic.

4. The contact resistance and contact thermal resistance between the bipolar plate and the gas diffusion layer are ignored.

5. Ignoring the influence of gravity on PEMFC.

Based on the above assumptions, the control equation of this paper is as follows :

Charge conservation equation:

$$\nabla\cdot\left(\sigma_{sol}\nabla\phi_{\mathrm{sol}}\right)+R_{\mathrm{sol}}=0 \tag{1}$$

$$\nabla\cdot\left(\sigma_{\mathrm{mem}}\nabla\phi_{\mathrm{mem}}\right)+R_{\mathrm{mem}}=0 \tag{2}$$

Where is σ_{sol} is solid phase conductivity, ϕ_{sol} is solid phase potential R_{sol} is solid phase volume transfer current, σ_{mem} is solid phase conductivity, ϕ_{mem} is solid phase potential, R_{mem} is solid phase volume transfer current.

Butler Volmer equation:

$$R_{\mathrm{an}}=\left(\zeta_{\mathrm{an}}\mathrm{j}_{\mathrm{an}}(T)\right)\left(\frac{[A]}{[A]_{\mathrm{ref}}}\right)^{\gamma_{\mathrm{an}}}\left(\mathrm{e}^{\alpha_{\mathrm{an}}^{\mathrm{an}}F\eta_{\mathrm{an}}/RT}-e^{-\alpha_{cat}^{an}F\eta_{an}/RT}\right) \tag{3}$$

$$R_{cat}=\left(\zeta_{cat}\mathrm{j}_{cat}(T)\right)\left(\frac{[C]}{[C]_{\mathrm{ref}}}\right)^{\gamma_{cat}}\left(\mathrm{e}^{\alpha_{\mathrm{an}}^{cat}F\eta_{cat}/RT}+e^{-\alpha_{cat}^{cat}F\eta_{cat}/RT}\right) \tag{4}$$

Where $\mathrm{j}_{\mathrm{an}}(T)$ is Anode reference exchange current density, ζ_{an} is Anode specific active surface area, $[A]$ is Anode hydrogen concentration. $[A]_{\mathrm{ref}}$ is Anode hydrogen reference concentration.; γ_{an} is anode hydrogen reference concentration. $\alpha_{\mathrm{an}}^{\mathrm{an}}$ is anode transfer coefficient of anode electrode; α_{cat}^{an} is cathodic transfer coefficient of anode electrode, F is faraday constant, R is ideal gas constant, T is working temperature, $\mathrm{j}_{cat}(T)$ is anode reference exchange current density, ζ_{cat} is cathode specific active surface area $[C]$ is cathode hydrogen concentration, $[C]_{\mathrm{ref}}$ is cathode hydrogen reference concentration, γ_{cat} is anode concentration ratio factor, $\alpha_{\mathrm{an}}^{cat}$ is anode transfer coefficient of cathode electrode, α_{cat}^{cat} is cathode transfer coefficient of the cathode electrode.

equation of mass conservation:

$$\frac{\delta(\varepsilon\rho)}{\delta\mathrm{t}}+\nabla\cdot\left(\varepsilon\rho\vec{u}\right)=S_m \tag{5}$$

Where ε is porosity of porous media, ρ is reaction gas density in the flow, $\vec{u}$ is reaction gas velocity vector in the flow channel, S_m is quality source items.

momentum equation:

$$\frac{\delta\left(\varepsilon\rho\vec{u}\right)}{\delta \mathrm{t}}+\nabla\left(\varepsilon\rho\vec{u}\vec{u}\right)=-\varepsilon\nabla p+\nabla\left(\varepsilon\mu\nabla\vec{u}\right)+S_{\mathrm{u}} \tag{6}$$

Where p is reaction gas pressure in the flow channel, μ is dynamic viscosity of reaction gas in flow channel, S_{u} is momentum source term.

Energy conservation equation:

$$\frac{\delta\left(\varepsilon\rho C_{\mathrm{p}}T\right)}{\delta \mathrm{t}}+\nabla\left(\varepsilon\rho C_{\mathrm{p}}\vec{u}T\right)=\nabla\left(\mathrm{k}^{\mathrm{eff}}\nabla\vec{\mathrm{u}}\right)+S_{\mathrm{h}} \tag{7}$$

$$S_{\mathrm{h}}=\mathrm{h}_{\mathrm{recat}}-R\eta+I^{2}R_{\mathrm{ohm}}+\mathrm{h}_{L} \tag{8}$$

where C_{p} is specific heat capacity, $\mathrm{k}^{\mathrm{eff}}$ is effective thermal conductivity, S_{h} is energy source term, $\mathrm{h}_{\mathrm{recat}}$ is net enthalpy change; R_{ohm} is ohmic resistance rate, h_{L} is entropy change.

Component conservation equation:

$$\frac{\delta\left(\varepsilon \mathrm{c}_{\mathrm{i}}\right)}{\delta \mathrm{t}}+\nabla\left(\varepsilon\vec{u}\mathrm{c}_{\mathrm{i}}\right)=\nabla\left(\mathrm{D}_{\mathrm{i}}^{\mathrm{eff}}\nabla \mathrm{c}_{\mathrm{i}}\right)+S_{\mathrm{i}} \tag{9}$$

Where c_{i} is constituent concentration, $\mathrm{D}_{\mathrm{i}}^{\mathrm{eff}}$ is effective diffusion coefficient of components; S_{i} is component source term.

3 Model validation is mesh independent

3.1 Model verification

In order to verify the reliability of the mathematical model proposed in this paper, The three dimensional isothermal multiphase DC channel established in reference[9] is used for verification. The SIMPLE algorithm is used to solve the problem, and the double precision solution method is used to calculate. It can be seen from Fig 4 that the simulation results of the mathematical model in this paper are in good agreement with the results in reference[9].Therefore, the mathematical model in this paper is accurate and reliable, and can be popularized in the numerical simulation of the flow channel of the pseudo serpentine plate of the magic mantis.

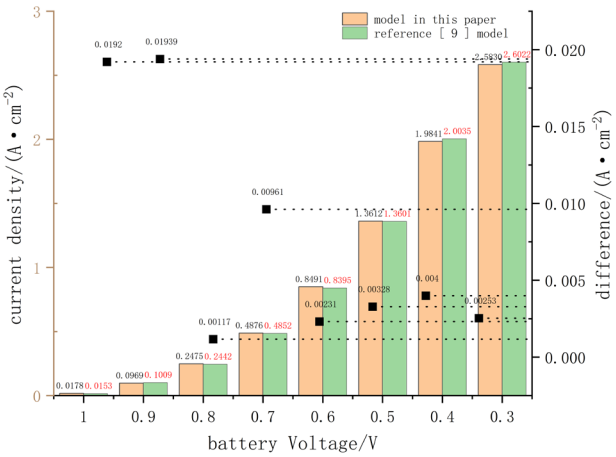

Fig. 4. model verification

3.2 Grid independence verification

The accuracy of the solution is related to the number of grid elements [10]. The main purpose of this study is to analyze the performance differences between the magic mantis pseudo snake plate with different flow channel sections and the traditional single channel snake plate. The number of grid elements at these locations needs to be gradually refined according to the calculation time and solution accuracy to determine the optimal number. The results of four cases with different grid numbers in the serpentine plate flow channel of the traditional model are analyzed : 400040,760086,1160048,1600028 and 1840032. The error analysis of the model with different grid numbers is shown in *Table 1*. The numerical model is carried out on a 48 core and 48 thread Intel Xeon microprocessor Gold 5318Y 2.6 GHz workstation with 64 GB RAM. At the same time, the simulation results of the battery voltage of 0.6 V were analyzed by evaluating the relative error of the current density under different grid numbers. After comparative analysis, it is found that the relative error is low in the model with the number of grids of 1600028 and 1840032. Based on this finding, in order to ensure a certain calculation accuracy while reducing the calculation cost and calculation time, 16,00028 grids are selected for subsequent numerical calculation, which balances the calculation accuracy and calculation efficiency to a certain extent, and provides reliable numerical calculation results.

Table 1

Model error analysis of different number of grids

mesh subdivision	grid number	current density /(A·m^{-2})	relative error
coarseness	400040	42.0821	—
routine	760086	43.0429	2.283
More detailed	1160048	44.2460	2.795
thinning	1600028	44.5621	0.714
refinement	1840032	44.86539	0.680

4 Results Analysis and Discussion

4.1 Feasibility and advantages

Fig 5 is the polarization curve and power density curve of the magic mantis pseudo snake plate and the traditional single channel snake plate. Fig 6 is the peak point of different channel cross sections of the magic flower mantis pseudo snake plate and the growth rate compared to the single channel snake plate. It can be seen from the curve that under the same flow channel volume, the magic mantis pseudo snake plate under different flow channel sections has better performance than the single channel snake plate. Due to the irreversible dynamics inside the fuel cell, including electrochemical reaction, proton transport, oxygen and fuel diffusion, the actual output voltage will be lower than the theoretical reversible voltage. These irreversible processes will cause the actual output voltage of the fuel cell to fail to reach the ideal reversible voltage[11]. Therefore, in practical applications, it is necessary to consider the effects of these irreversible processes on the performance of fuel cells and optimize and improve them accordingly to improve the efficiency and stability of fuel cells[12]. In fact, there are other causes of loss, divided into polarization loss, ohmic loss and mass transfer loss[13], Through observation, it is found that when the voltage is greater than 0.6V, the slope of the polarization curves of the two is relatively close. At this time, the battery is in the activation loss and ohmic loss region, indicating that the internal electrochemical reaction rate of the two is basically proportional. When the voltage is less than 0.6V, the battery is in the mass transfer loss area, and the slope of the polarization curve of the single channel snake shaped plate decreases sharply, while the slope of the polarization curve of the magic mantis pseudo snake shaped plate with different flow channel sections is in turn. The slope of the gentle decline, in which the pentagonal flow channel cross section of the magic mantis pseudo snake shaped plate increases the most, the peak current increases by 33.23 %, and the peak power increases by 23.64 %. This is because at high current density, the flow channel of the magic mantis pseudo snake shaped plate is faster than the flow channel of the snake shaped plate, allowing the gas reactant to be quickly transferred to the catalytic layer.

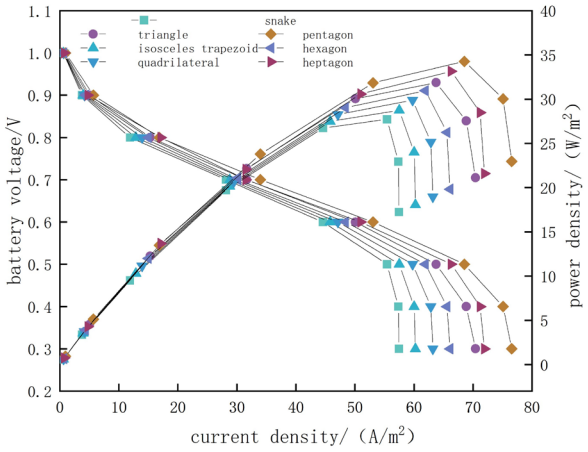

Fig. 5. The polarization curve and power density curve of the pseudo serpentine plate flow channel and the serpentine plate flow channel of the magic flower mantis

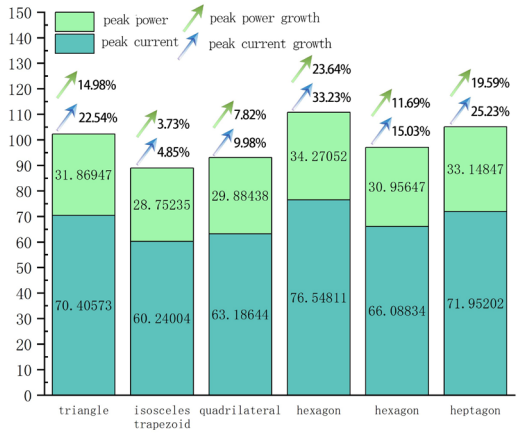

Fig. 6. Magic flower mantis pseudo snake plate peak of different flow channel

4.2 Local distribution and transport characteristics of flow channel

4.2.1 Oxygen concentration and water distribution in cathode flow channel

Fig 7 shows the distribution of cathode O_2 molar concentration. It is found that the O_2 concentration of the gas flow channels of the two plates decreases from the inlet to the outlet. It can be seen from the diagram that the oxygen distribution in the front section of the serpentine plate flow channel is uneven and the concentration is low, resulting in a decrease in the electrochemical reaction

efficiency. The oxygen distribution in the front section of the pseudo snake plate flow channel of the magic flower mantis is uniform. Among them, the oxygen in the front section of the pentagonal section flow channel reaches 2.97 mol/m^3, which is much larger than the oxygen concentration in the front section of the serpentine plate flow channel. At the same time, the distribution of O_2 in the pseudo snake plate flow channel of the magic flower mantis is significantly more than that of the serpentine plate flow channel. The structural advantages of the internal flow channel also make the internal reaction gas concentration more balanced, and there will be no scattered distribution of oxygen concentration in the longitudinal YZ section. Therefore, the magic flower mantis pseudo snake plate flow channel will have a greater concentration difference, which is conducive to the transmission of O_2 in the flow channel. When the battery enters the mass transfer loss area, the voltage loss caused by the decrease of the reactant concentration is smaller, while the mass transfer polarization in the serpentine plate flow channel is severe, resulting in a large voltage loss and a decrease in current density[14]. Fig 8 shows the water distribution in the cathode channel. The water generated by the electrochemical reaction at the cathode and the electroosmotic drag effect lead to the uneven distribution of water inside the fuel cell. Since the electrochemical reaction produces more water at the cathode, the electroosmotic drag will bring more water from the anode to the cathode, resulting in a more concentrated water distribution in the cathode area and a sparse water distribution in the anode area. This uneven water distribution will affect the performance and stability of the fuel cell, so corresponding optimization and improvement are needed to achieve a more uniform water distribution.

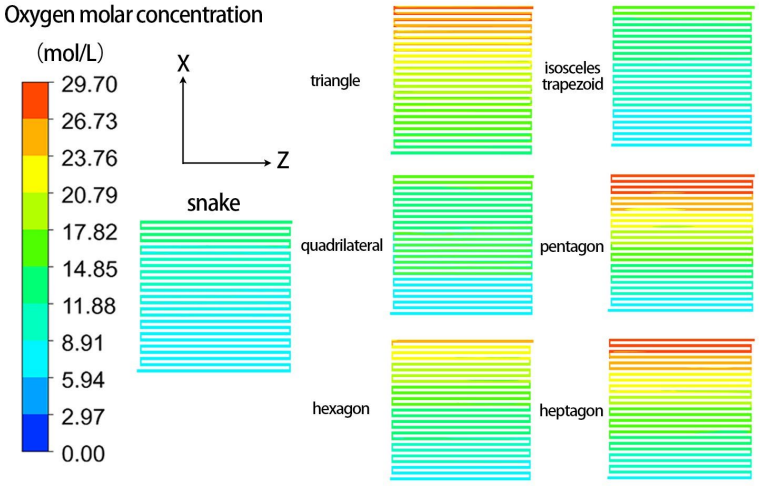

Fig. 7. Molar concentration distribution of O_2 in cathode channel

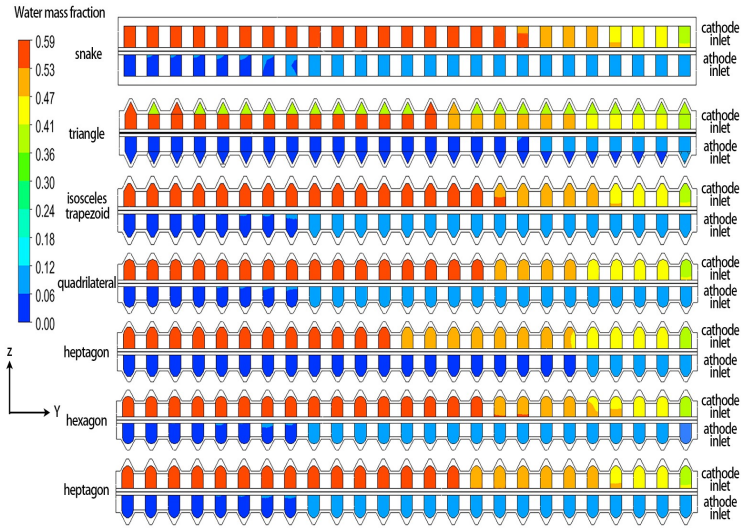

Fig. 8. Mass fraction of water in cathode flow channel

The mass fraction of water in the two channels is proportional to the distribution of O2 molar concentration. After the gas enters, water begins to be produced inside the battery, and the reaction gas can take away part of the water. As the gas gradually deepens, the proportion of water in the channel gradually increases. This phenomenon is due to the continuous production of water by the electrochemical reaction at the cathode, and the water will gradually accumulate and accumulate during the flow process in the flow channel. Therefore, in the cathode flow channel, from the inlet to the outlet, the moisture content will gradually increase. This increase in moisture can affect the performance and stability of the fuel cell, and needs to be optimized and regulated accordingly. It can be seen from Fig 8 that the water content of the pseudo serpentine plate of the magic mantis with different flow channel sections is lower than that of the serpentine plate. The water content of the triangular flow channel section and the pentagonal flow channel section is relatively low, indicating that the pseudo serpentine plate of the magic mantis can change the trajectory of the liquid water generated by the chemical reaction in the flow channel. Therefore, better drainage capacity can effectively reduce the phenomenon of water accumulation in the flow channel, and ultimately ensure the water management balance of the fuel cell and will not reduce the mass transfer efficiency of the fuel cell, thereby improving the performance and stability of the fuel cell.

4.2.2 Water distribution in gas diffusion layer

Fig 9 is the water distribution diagram of the cathode gas diffusion layer. The proton conductivity of the proton exchange membrane is closely related to the water content. Only when the water is sufficient can it be guaranteed to have a

high proton conductivity. The water of the proton exchange membrane mainly comes from the internal generated water. As the working current density gradually increases, the rate of water generation also increases accordingly. Only the water in the membrane binding state can effectively improve the proton conductivity of the fuel cell, and too much liquid water will occupy the pores in the gas diffusion layer[15].It hinders the diffusion of gas, hinders the transmission of reaction gas to the reaction point, produces the phenomenon of ' flooding ', and seriously reduces the performance of the battery. By comparing with the serpentine plate flow channel, it is found that the gas reaction area is reduced at the corner of the serpentine plate flow channel, and the water transport efficiency in the flow channel is further improved. After multiple corner acceleration, it can effectively solve the problem of water flooding. Among them, the water distribution in the gas diffusion layer of the pentagonal section is the most uniform, maintaining at about 7.96 mol/m^3.

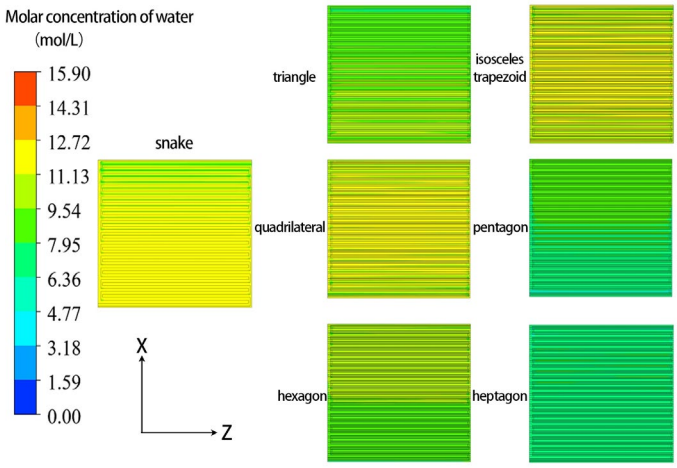

Fig. 9. Water distribution in cathode gas diffusion layer

5 Conclusion

To study the improvement of PEMFC performance by the magic mantis pseudo snake plate, this paper conducts modeling and simulation research on the snake plate and the magic mantis pseudo snake plate with six different flow channel sections. By analyzing the polarization curve, the cathode flow channel O_2 molar concentration distribution, the cathode flow channel water distribution, the cathode flow channel temperature, the cathode flow channel pressure drop and the cathode gas diffusion layer water distribution, the following conclusions are drawn:

1. The flow channel of the magic mantis pseudo snake plate effectively improves the current density of PEMFC and promotes the stable internal electrochemical reaction. Compared with the flow channel of the snake plate with the same flow channel volume, the peak current density of the magic mantis pseudo snake plate with pentagonal flow channel section increases by 33.23%, and the peak power increases by 23.64%.

2. Compared with the traditional single serpentine plate flow channel, the magic mantis pseudo serpentine plate flow channel can reduce the battery temperature by about 3 degrees Celsius, avoid thermal runaway inside the battery, and effectively extend the life of each component of the battery.

3. The corner of the pseudo snake plate flow channel of the magic mantis narrows the reaction gas channel, so that the overall pressure is higher than that of the single snake plate flow channel, which is conducive to the diffusion of the reaction gas in the flow channel, and the water in the flow channel is quickly discharged. The water deposition in the flow channel delays the concentration polarization and significantly improves the output performance of the fuel cell.

4. With the change of the cross section of the pseudo serpentine plate channel of the magic mantis, the output current density and power density of the battery show a trend of increasing first and then decreasing. When the battery voltage is 0.6V, the peak current and peak power of the pentagonal section are the largest, which are 76.54811 A/m^3 and 34.27052 W/m^2, and the peak current and peak power of the isosceles trapezoid section are the smallest, which are 60.24004 A/m^3 and 28.75235 W/m^2.

The transmission of reaction gas in the flow channel and the removal of water in the flow channel of the pseudo serpentine plate of the mantis have been significantly improved. The liquid water content in the cathode flow channel of the pseudo serpentine plate of the mantis with pentagonal flow channel section is reduced by 26.23%, and the membrane water content of the gas diffusion layer is reduced by 31.2%.

REFERENCES

[1]. *S. T. Bunyan, H. A. Dhahad, D. S. Khudhur, and T. Yusaf*, Sustainability 15, 10389,2023.
[2]. *G. Zhang, Z. Qu, W. Q. Tao, X. Wang, L. Wu, S. Wu, X. Xie, C. Tongsh, W. Huo, Z. Bao, K. Jiao, and Y. Wang*, Chem. Rev. 123, 989,2023.
[3]. *Y. Zou, S. Hua, H. Wu, C. Chen, Z. Wei, Z. Hu, Y. Lei, J. Wang, and D. Zhou*, Energies 16, 5932,2023.
[4]. *X. Xie, B. Yin, S. Xu, H. Jia, F. Dong, and X. Chen*, International Journal of Hydrogen Energy 47, 3473,2022.
[5]. *Q. Tan, H. Lei, and Z. Liu*, International Journal of Hydrogen Energy 47, 11975,2022.
[6]. *T. Huang, W. Wang, Y. Yuan, J. Huang, X. Chen, J. Zhang, X. Kong, Y. Zhang, and Z. Wan*, Energy Reports 7, 1374,2021.

[7]. *M. Fan, F. Duan, T. Wang, M. Kang, B. Zeng, J. Xu, R. Anderson, W. Du, and L. Zhang*, Energies 14, 1250,2021.
[8]. *W. Wanteng, L. Nan, X. Hongpeng, X. Ruiyang, Zhang Jinhui,* Journal of Solar Energy 43, 448, 2022.
[9]. *P. Lin, H. Wang, G. Wang, J. Li, and J. Sun*, International Journal of Hydrogen Energy 47, 5541,2022.
[10]. *S. Feng, S. Dandan, Y. Yujie, D. Xiaoping, L. Zhiyuan, and P Bin,* Journal of Solar Energy 43, 414, 2022.
[11]. *P. Dong, G. Xie, and M. Ni*, *Energy* 206, 117977,2020.
[12]. *W. Ke, Z. Shuyang, X. Hongtao, L. Shun, and M. Yijun,* Journal of Solar Energy 43, 454, 2022.
[13]. *C. Chen, C. Wang, and Z. Zhang*, *Energy* Conversion and Management 254, 115273,2022.
[14]. *Y. Li, J. Bi, M. Tang, and G. Lu*, Micromachines 13, 665,2022.
[15]. *L. Yuting, L. Gui, and L. Yuanyuan,* Journal of Engineering Thermophysics 41, 2900, 2020.